

CHEMISTRY

A European Journal

A Journal of



Accepted Article

Title: Syntheses of Exceptionally Stable Al(III) Metal-Organic Frameworks: How to Grow High Quality Large Single Crystals?

Authors: Ya-Qian Lan, Yuanyuan Guo, Jun Zhang, Longzhang Dong, Yan Xu, Wei Han, Min Fang, Hong-Ke Liu, and Yong Wu

This manuscript has been accepted after peer review and appears as an Accepted Article online prior to editing, proofing, and formal publication of the final Version of Record (VoR). This work is currently citable by using the Digital Object Identifier (DOI) given below. The VoR will be published online in Early View as soon as possible and may be different to this Accepted Article as a result of editing. Readers should obtain the VoR from the journal website shown below when it is published to ensure accuracy of information. The authors are responsible for the content of this Accepted Article.

To be cited as: *Chem. Eur. J.* 10.1002/chem.201703682

Link to VoR: <http://dx.doi.org/10.1002/chem.201703682>

Supported by
ACES

WILEY-VCH

Syntheses of Exceptionally Stable Al(III) Metal-Organic Frameworks: How to Grow High Quality Large Single Crystals?

Yuanyuan Guo,^{†[a]} Jun Zhang,^{†[b]} Long-Zhang Dong,^[a] Yan Xu,^[c] Wei Han,^[a] Min Fang,^{*[a][d]} Hong-Ke Liu,^{[a][d]} Yong Wu^{*[a]}, Ya-Qian Lan^{*[a]}

Abstract: The difficulty of obtaining large single crystals of aluminum carboxylate MOFs (Al-MOFs) for structure determinations has limited the development of these water and thermally stable MOFs. In this work, how large single crystals of the known MIL-53(Al) and the first two tetrahedral ligand based, visible light absorbing 3D Al-MOFs, $[\text{Al}_3(\text{OH})_3(\text{HTCS})_2]$ (**AITCS-1**) and $[\text{Al}_5\text{O}_2(\text{OH})_3(\text{TCS})_2(\text{H}_2\text{O})_2]$ (**AITCS-2**) (TCS = tetrakis(4-oxycarbonylphenyl) silane) are obtained in the presence of hydrofluoric or formic acid for conventional single-crystal diffraction measurements is presented, demonstrating a general method of obtaining large and good quality single crystals of Al-MOFs. **AITCS-1** and **-2** can be stable in a wide pH range (1-11), and **AITCS-1** can even be stable in aqua regia solution for at least 24 h. The BET specific surface area of **AITCS-1** and **-2** are 11 and 1506 m² g⁻¹, respectively. **AITCS-2** uptakes 51 cm³ (STP)/g CO₂ and 15 cm³ (STP)/g CH₄ at 298 K and 1 bar, which is relatively high among MOF materials. **AITCS-1** uptakes 30 cm³ g⁻¹ CO₂ and 4.2 cm³ g⁻¹ CH₄ at 298 K and 1 bar. The rapid and stable photocurrent responses of **AITCS-1** and **-2** under UV and visible light illuminations are observed. Moreover, **AITCS-1** photocatalyzes the water-splitting reaction under visible light with an average hydrogen evolution efficiency of 50 μmol·g⁻¹·h⁻¹ for the first 10 h in a mixed solvent of water and triethanolamine.

Introduction

Visible light is the major component (43%) of the inexhaustible and clean solar energy. Metal-organic frameworks (MOFs) can be synthesized as visible light photocatalysts due to their designability.^[1] However, relatively low water and thermal stabilities of most MOFs could be the key limitations for their practical applications.^[2] Al-MOFs show exceptionally water and thermal stability. They are relatively light due to the low atomic number of Al. Although not many of Al-MOFs are reported, they have become of interest for industrial uses.^[3] To the best of our knowledge, only two MOFs have been promoted to the level of commercial applications. A dense zinc glutarate^[4] is currently used as an epoxide-polymerization catalyst, while the microporous aluminum fumarate A520 is employed as a sorbent to store and deliver natural gas for automotive applications.^[3, 5] Up to now, the total number of structures of Al-MOFs is only 42 (Table S1 and Table S2 in Supporting Information (SI)), among which only 16 structures are based on single crystal XRD diffraction analyses (Table S2). Due to the small sizes, 9 of the 16 single crystal XRD diffractions were performed using synchrotron radiations, which are not readily accessible to researchers. Therefore, it is necessary to find a general method

to obtain single crystals of Al-MOFs for common XRD structure determination. In addition, no tetrahedral shape carboxylic acid ligand has been applied in the syntheses of Al-MOFs.

Loiseau *et al.* first applied HF aqueous solution to synthesize single crystals of an Al-MOF (MIL-96) in 2006.^[6] They also utilized tetraethylortho silicate (Si(OC₂H₅)₄, TEOS) and trimethyl 1,3,5-benzenetricarboxylate (C₆H₃(CO₂CH₃)₃), an ester ligand instead of the acid ligand to facilitate the formation of Al-MOFs. Since then, no single crystals of Al-MOFs were reported by adding HF acid. The method of adding HF aqueous solution to growth large crystals has been applied in related fields. For example, large single crystals of AlPO₄-34, a molecular sieve, was synthesised by adding HF aqueous solution.^[7] Guo *et al.* reported that the irregular particles of UiO-66, a Zr(IV) carboxylate MOF changed into regular shaped particles and the sizes increased from 0.2-0.5 to 5-10 μm through adding HF acid.^[8] Simple organic acids were also applied in synthesizing MOF single crystals, especially in the syntheses of Zr-MOFs.^[9] Despite of all the above progresses, obtaining large single crystals of an Al-MOF is still a difficult task.

In this paper, single crystals of the known MIL-53(Al) (previously obtained as powders), and two novel Al-MOF crystals, $[\text{Al}_3(\text{OH})_3(\text{HTCS})_2]$ (**AITCS-1**) and $[\text{Al}_5\text{O}_2(\text{OH})_3(\text{TCS})_2(\text{H}_2\text{O})_2]$ (**AITCS-2**), big enough for conventional single-crystal diffraction measurements are obtained by adding HF aqueous solution or formic acid, demonstrating a general method for obtaining high quality large single crystals of Al-MOFs. The syntheses, structures, chemical and thermal stabilities, gas adsorptions, photocatalytic water splitting, photoelectric properties of **AITCS-1** and **-2** are reported. Although H₄TCS ligand absorbs only UV light, **AITCS-1** and **-2** absorbs visible light, and **AITCS-1** absorbs more visible light than **AITCS-2**. Their band gaps, and CB- and VB-edge positions were determined using UV-Vis reflectance spectra and an electrochemical method. **AITCS-1** photocatalyzes the water splitting with a hydrogen evolution efficiency of 50 μmol·g⁻¹·h⁻¹ for the first 10 h in a mixed solvent of water and triethanolamine (4:1 volume ratio).

[a] YuanyuanGuo, Longzhang Dong, Dr. Wei Han, Prof. Min Fang, Prof. Ya-Qian Lan, Prof. Hong-Ke Liu, Dr. Yong Wu
Department of Chemistry
Nanjing Normal University, Nanjing 210023, China
Email:fangmin@njnu.edu.cn, wuyong@njnu.edu.cn, yqlan@njnu.edu.cn

[b] Dr. Jun Zhang
Anhui Key Laboratory of Advanced Building Materials
Anhui Jianzhu University, Hefei, Anhui 230022, China.

[c] Prof. Yan Xu
State Key Laboratory of Materials-Oriented Chemical Engineering
Nanjing Tech University, Nanjing 210009, China

[d] Prof. Min Fang, Prof. Hong-Ke Liu
State Key Laboratory of Coordination Chemistry
Nanjing University, Nanjing 210093, China

[†] These authors contribute equally to this paper.
Supporting information for this article is given via a link at the end of the document.CCDC 1523998 (**AITCS-1**),1523999 (MIL-53(Al single crystal), and 1551336 (**AITCS-2**).

Results and Discussion

Syntheses of the large single crystals of MIL-53(Al) and $[Al_3(OH)_3(HTCS)_2]$ (AITCS-1)

In order to obtain single crystals of new Al(III) carboxylate MOFs, we first tried to obtain the single crystal of a known Al-MOF, MIL-53(Al). A common $Al(NO_3)_3 \cdot 9H_2O : H_2BDC : H_2O$ molar ratio for the synthesis of MIL-53(Al) powder is 2.0 : 1 : 178.^[6] By simply adding HF aqueous solution to the above mixture (Table S7), the particles of MIL-53(Al) increases (Figure 1(a)-(b)), and eventually large block single crystals of 0.25 × 0.14 × 0.07 mm (Figure 1(c)) obtained using a HF : H_4TCS molar ratio of 4.4. The single-crystal structure was determined using the common single-crystal XRD diffraction analysis and consistent with that determined based on the PXRD data (Table S3, Figure S3 and S4).^[4] In 2015, Seoane *et al.* obtained MIL-53(Al) single crystals of the size of 0.8 × 0.9 × 0.4 μm ,^[10] which is not big enough for the structure determination using a common single-crystal XRD diffractometer.

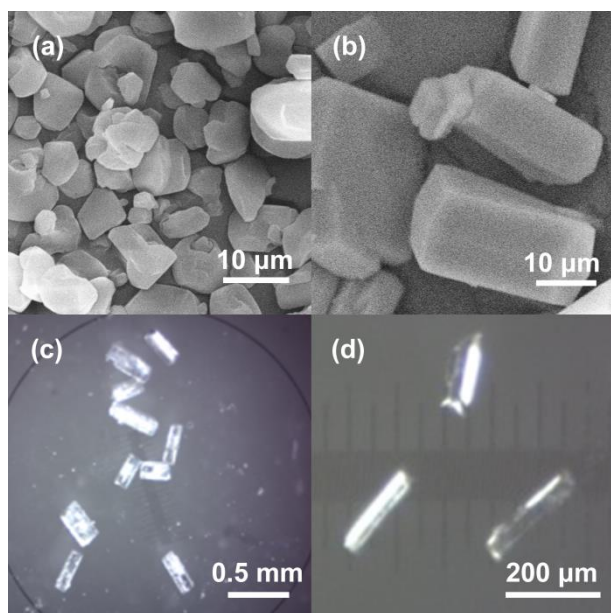


Figure 1. Morphologies of large single crystals of MIL-53(Al) (c) and AITCS-1 (d). The SEM images of products prepared using the same procedure of the synthesis of the MIL-53(Al) single crystal but using different HF : H_4TCS molar ratio (0.39 for (a), 2.3 for (b)) are also given for comparison.

To synthesize single crystals of a new Al(III)-MOF based on the H_4TCS ligand, the $L_9(3^4)$ orthogonal array design approach was applied.^[11] The $L_9(3^4)$ array gives 9 representative experiments considering 4 influencing factors and three different conditions for each factor. The factors we considered are the molar ratio of $Al(NO_3)_3 \cdot 9H_2O$ to H_4TCS (1:1, 1:2 and 1:3), the molar ratio of HF to H_4TCS (0, 1.1, 2.1), amounts of water (4.0, 6.0 and 8.0 mL) and the fourth factor was kept as the same (e.g. reaction time). The experiments designed by this method are given in Table 1. Other synthetic procedures are the same as that of the synthesis of the MIL-53(Al) single crystal except that the heating and cooling rates of the oven temperature were slowed down and controlled. The experimental results are listed

Table 1. The effect of the amounts of reactants on the syntheses of AITCS-1 using the 9 experiments designed using the $L_9(3^4)$ orthogonal array.^[a]

No.	The molar ratio of $Al(NO_3)_3 \cdot 9H_2O : H_4TCS : HF : H_2O$	Product (size in mm)
1	1 : 1 : 0 : 2850	Powder
2	1 : 1 : 1.1 : 4270	Small block crystals of AITCS-1
3	1 : 1 : 2.1 : 5700	Long needles (Figure S6(a))
4	2 : 1 : 0 : 4270	Powder
5	2 : 1 : 1.1 : 5700	Large block crystals of AITCS-1 (0.17 × 0.040 × 0.030) (Figure 1(d))
6	2 : 1 : 2.1 : 2850	Large block crystals of AITCS-1 (0.20 × 0.040 × 0.020)
7	3 : 1 : 0 : 5700	Powder
8	3 : 1 : 1.1 : 2850	Large block crystals of AITCS-1 (0.10 × 0.050 × 0.050) (Figure S5(c))
9	3 : 1 : 2.1 : 4270	Needles + AITCS-1 block crystals

[a] The amount of H_4TCS (40 mg, 0.078 mmol) was kept being constant and the other synthetic procedures and conditions were as the same as the typical synthesis of AITCS-1.

in Table 1. Large block-shape single crystals of a new phase were obtained in three experiments (No. 5, 6 and 8). One of the crystal was structurally determined by the single-crystal X-Ray diffraction analysis as $[Al_3(OH)_3(HTCS)_2]$ (denoted as AITCS-1). The above results demonstrate the efficiency of the orthogonal experimental design method. Just by 9 experiments, pure and large single crystals of AITCS-1 were harvested and the crystal structure was obtained using a common single-crystal XRD diffractometer. This systematic analysis tool is widely used in biochemistry and various fields of chemistry,^[12] however few reports were published in the field of coordination networks. By applying formic acid instead of HF aqueous solution, we also successfully obtained large single crystals of AITCS-1 using 10 mg (0.020 mmol) H_4TCS in each preparation (the overall molar ratio of $Al^{3+} : H_4TCS : HCOOH : H_2O = 3.9-6.5 : 1 : 680 : 17000$) (Table S8, Figure S6 and S7).

Syntheses of the high quality large single crystals of $[Al_5O_2(OH)_3(TCS)_2(H_2O)_2]$ (AITCS-2)

AITCS-1 has a low porosity 16.8% due to the pore filling effect of the -COOH containing arm of each ligand. In the following endeavors, we successfully obtained a novel Al-carboxylate MOF based on the completely deprotonated TCS^{4-} ligand, $[Al_5O_2(OH)_3(TCS)_2(H_2O)_2]$, which is denoted as AITCS-2. Selected experiments and results are given in Table 2, the corresponding PXRD results and pictures of the selected crystals given in Figure 2 and Figure 3. In the beginning, we obtained the powder phase of AITCS-2 (No. 1 in Table 2). We thought it was a potential target of a new Al-MOF since its PXRD pattern has a peak at low 2θ angle, 6.02° (No. 1 in Figure 2), which is smaller than the first PXRD peak of AITCS-1 (6.63°), suggesting it might have bigger pores than those in AITCS-1. Subsequently, in a more concentrated solution and with a slower heating and cooling rate of the oven, powders of higher crystallinity (No. 2 in Figure 2) were obtained as indicated by the intensity increase of the peak at 6.02° (from 1500 to 4500). Based on No. 2, by increasing the acidity of the system, using a more dilute reactant mixture and a faster cooling rate, rhombic crystals were obtained (No. 5-6 in Table 2), however the crystallinity is low (Figure 2). Raising the temperature from 120 to $130^\circ C$, we obtained perfect looking, large rhombic crystals (0.15 × 0.10 × 0.030 mm, No. 8 in Figure 3). Its PXRD diffraction intensity of the peak at 6.02° is high, but the peaks are broad,

Table 2. Syntheses of single crystals of AITCS-2.^[a]

No.	The molar ratio of Al ³⁺ :H ₄ TCS:HCOOH:DMF:H ₂ O ^[b]	Products (size in mm)
1 ^[d]	4.0 (293 mg) : 1.0 (10) : 680 (0.50) : 2660 (4.0) : 0	AITCS-2 , powder
2 ^[c]	6.0(351) : 1.0(30) : 226 (0.5) : 443 (2) : 0	AITCS-2 , powder
3	6.0 (234) : 1.0(20) : 374 (0.55) : 670 (2) : 0	Phase C , glassy particles
4	5.8 (227) : 1.0(20) : 340(0.5) : 670 (2) : 0	Phase C , rhombic crystals, (0.040x0.030x0.010) (Figure S8)
5 ^[c]	6.0 (234) : 1.0(20) : 340 (0.5) : 670 (2) : 0	AITCS-2 , rhombic single crystals
6	6.0 (117) : 1.0(10) : 680 (0.5) : 1990 (3) : 0	AITCS-2 , rhombic single crystals (0.14 x0.10x0.040)
7 ^[c]	6.0 (117) : 1.0(10) : 1090 (0.8) : 1990 (3) : 0	Phase D , glassy particles
8 ^[e]	5.8 (227) : 1.0(20) : 340 (0.5) : 670(2) : 0	AITCS-2 , rhombic single crystals (0.15 x0.10x0.030)
9	5.8 (227) : 1.0(20) : 270 (0.4) : 500 (1.5) : 710 (0.5)	AITCS-2 , block-like single crystals (0.20x0.10x0.030)
10 ^[c]	5.8 (227):1.0(20) : 270 (0.4) : 500 (1.5):710(0.5)	AITCS-2 , block-like single crystals (0.28 x0.12 x0.045)
11	5.8(227) : 1.0(20) : 310 (0.45) : 500 (1.5):710 (0.5)	AITCS 2 , block-like single crystals (0.20x0.10x0.020)
12 ^[d]	5.8 (227) : 1.0(20) : 310 (0.45) : 500 (1.5):710(0.5)	AITCS-2 , block-like single crystals (0.15 x0.08 x0.020)
13	5.8 (227) : 1.0(20) : 270 (0.4) : 470 (1.4) : 850 (0.6)	AITCS-2 , block-like single crystals (0.20x0.10x0.020)
14 ^[d]	5.8 (227) : 1.0(20) : 270 (0.4) : 470 (1.4):850 (0.6)	AITCS-2 , block-like single crystals (0.08 x0.030 x0.015)

[a] PXRD patterns are given in Figure 2 and pictures of selected products are given in Figure 3; [b] Data in parentheses are the amount of Al(NO₃)₃ aq. (1.0 M, μL) (except for No. 1 in which solid Al(NO₃)₃·9H₂O was applied), H₄TCS (mg), HCOOH (mL), DMF (mL) and H₂O (mL). The total volume of DMF and H₂O are 2.0 mL except for No. 1 in which 4 ml of DMF was applied; the temperature of the oven was raised from room temperature to 120 °C with a 1.0 °C/min heating ramp, kept at 120 °C for 3 d, and then cooled to 25 °C with a rate of 10.0 °C/h. [c] Same as [b] except that the cooling rate is 2.0 °C/h to 25 °C; [d] The autoclave was put into an oven, and the temperature of the oven increased from 25 to 120 °C naturally, kept at 120 °C for 3 d and then cooled to room temperature naturally; [e] Reaction temperature is 130 °C, heating ramp and cooling rate are the same as [b].

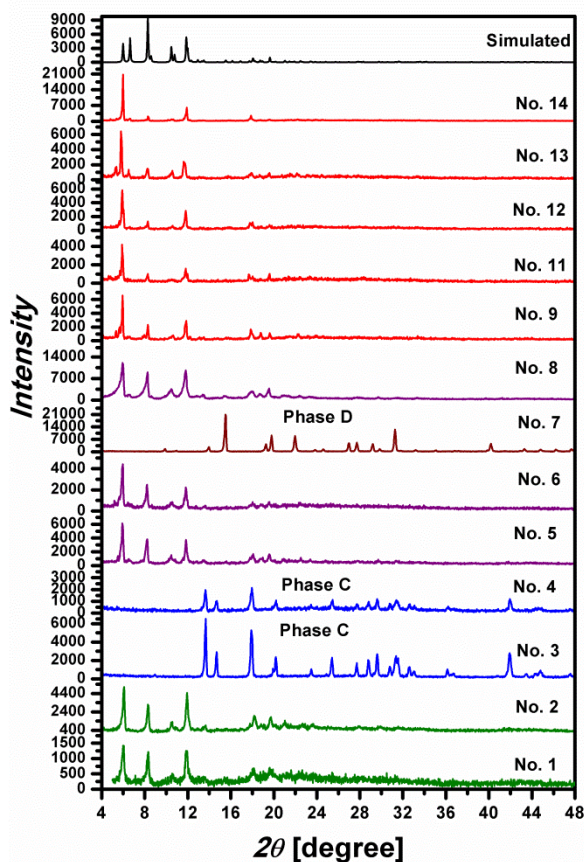


Figure 2. The PXRD patterns of AITCS-2, phase C and Phase D produced from experiments given in Table 2, compared with the simulated PXRD patterns based on the cif file of AITCS-2 using Mercury software.

indicating that there exist disorders in the crystals causing the broadening of the peaks. Only a few or no single crystal XRD diffraction points were observed from all rhombic crystals obtained in DMF. Increasing the acidity of the system and cooling rate (10 °C/h) resulted in a dense phase (**Phase C**, No. 3 and 4). This phase can also be obtained as rhombic crystals (No. 4, Figure S8). Even higher acidity resulted in another dense phase (**Phase D**, No. 7).

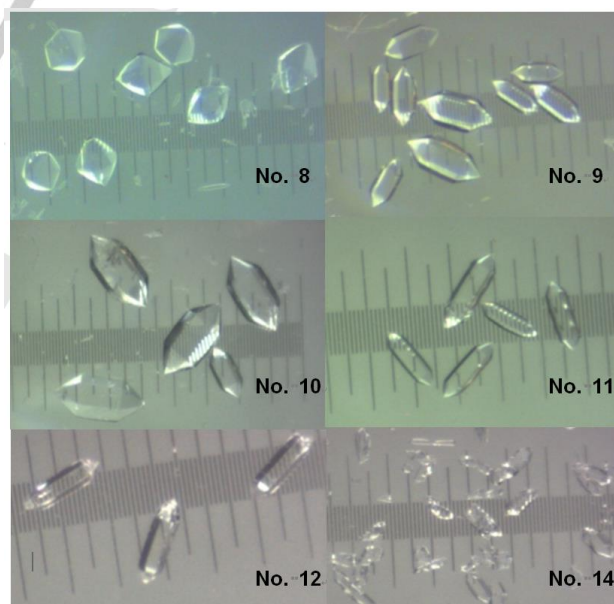


Figure 3. Pictures of the synthesized AITCS-2 single crystals by the experiments given in Table 2. The length of the minimum grade in the pictures is 0.01 mm.

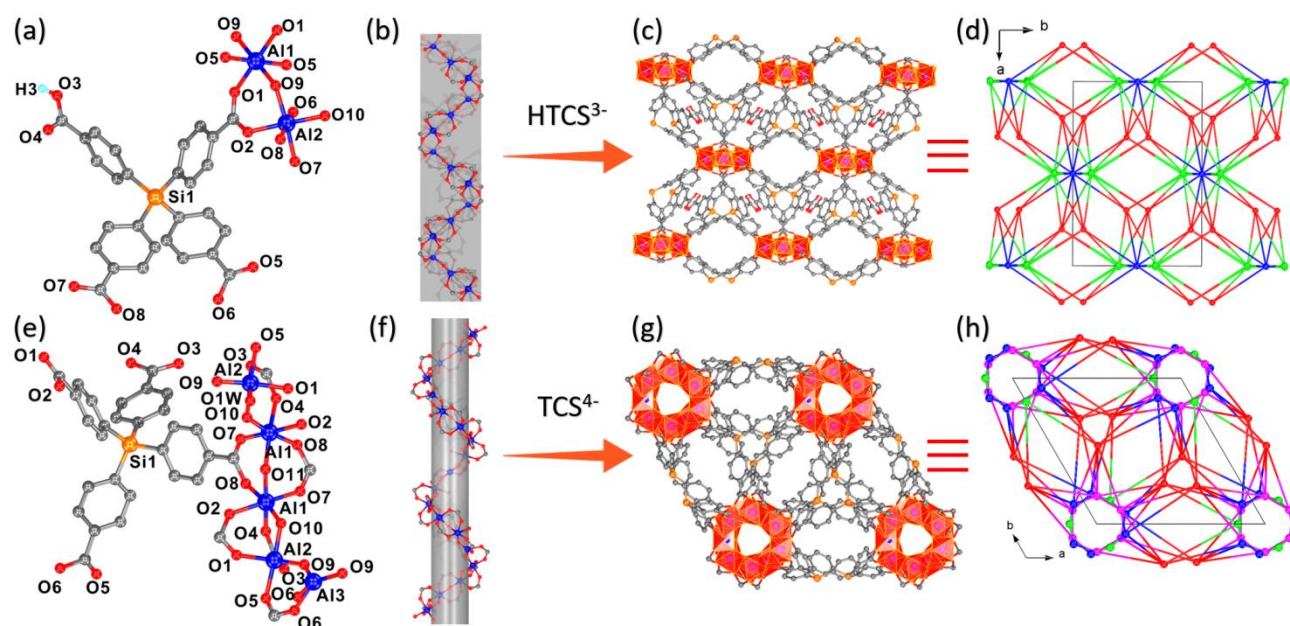


Figure 4. The structures of **AITCS-1** ((a)-(d)) and **AITCS-2** ((e)-(h)). The coordination environments ((a) and (e)), the Al^{3+} chains ((b) and (f)), the packings along *c* axis ((c) and (g)), and the topologies ((d) and (h)) are given.

To grow better quality crystals of **AITCS-2**, we then changed the polarity of the solvent by using mixed solvents of DMF and H_2O . The total amount of the solvent was kept at 2.0 mL to maintain the concentration. Block-like crystals were obtained in this system (No. 9-14 in Table 2, Figure 2-3). Contrary to our expectation, it was found that increasing the cooling rate would increase the crystallinity of **AITCS-2** (No. 14 versus No. 13; No. 12 versus No. 11). The diffraction intensity of the peak at 6.02° of the No. 14 product reaches 21000 and the peaks are very sharp. Only with single crystals of this experiment, we obtained good diffraction data with a qualified resolution and the single crystal structure of **AITCS-2** was solved. Data obtained from other block-like crystals all have poor resolutions (> 1.0). Tsao *et al.* also found that high-quality MOFs can be synthesized as the cooling rate increases.^[13] In the synthesis of **AITCS-1**, we also found that faster cooling rate would increase its crystallinity (Figure S17).

The position of the simulated PXRD pattern of **AITCS-2** based on the crystal structure is consistent with the observed patterns; however the intensities were different (Figure 2). This could be due to the crystal for the structure determination was measured with solvents inside the pores, however the observed PXRDs were obtained after the samples were dried $60\text{--}90^\circ\text{C}$ for 12 h. The peak intensities of the PXRD pattern of a sample which was soaked in water for three days (Figure 7(b)) are more consistent with the simulated PXRD pattern based on the crystal structure. Thus phenomena have been observed by us and others.^[14] Intensity differences between observed patterns are probably due to the different orientation preferences of prepared **AITCS-2** since we have prepared them in different shapes. Some small additional peaks at the low angles are probably due to small amounts of impurities.

Structures of **AITCS-1** and -2

The minimum unsymmetrical units of **AITCS-1** and -2 are given in Figure S9. Single-crystal X-ray diffraction analysis reveals that **AITCS-1** has a 3D framework, crystallizes in the monoclinic space group $C2/c$ (Table S3). The coordination

environments of the ligand and metal ions of **AITCS-1** are shown in Figure 4(a). The carboxylate groups all act as bidentate ligands, bridging two adjacent $\text{Al}(\text{III})$ ions. Six coordinated Al^{3+} ions (Al1 and Al2) are bridged by carboxylate groups and OH^- groups to form zig-zag planar chains along *c* axis as shown in Figure 4(b). 29 out of the total 42 Al-MOF structures contain 1-D metal oxide chains (Table S1 and Table S2). However, only MIL-96,^[6] 467-MOF^[15] contains zig-zag chains as those in **AITCS-1**. The chains are connected by HTCS^{3-} ligands forming a 3D framework, showing rhombic channels of $6.4(4.7) \times 9.1(7.4) \text{ \AA}^{[41]}$ along *c* axis (Figure 4(c) and Figure S10). The unprotonated arm of H_4TCS has filled the pores of **AITCS-1**, making it having a small porosity of 16.8% (probing radius: 1.2 \AA) and the solvent accessible volume/unit cell: 995.2 \AA^3 as calculated by the PLATON program.^[16] The pore volume calculated based on the above data is $0.13 \text{ cm}^3/\text{g}$. Based on the topology analysis using ToposPro program,^[17] the 3D framework of **AITCS-1** can be simplified as a 3-nodal 6,6,6-*c* net ($(\text{Si}_2(\text{Al1})(\text{Al2})_2)$ with a point symbol of $(3^3 4^2 5^7 6^3)_2 (3^4 4^2 5^2 6^4 7^2 8)$ ($3^4 4^5 5^4 6^3$)₂ as shown in Figure 4(d). To the best of our knowledge, this is a new topology.

Single-crystal X-ray diffraction analysis reveals that **AITCS-2** ($[\text{Al}_5\text{O}_2(\text{OH})_3(\text{TCS})_2(\text{H}_2\text{O})_2]$) is a 3D framework, crystallizes in the trigonal space group $P3_12_1$ (Table S4). All carboxylate groups act as bidentate ligands, bridging two adjacent $\text{Al}(\text{III})$ ions as in **AITCS-1**. Al^{3+} ions (Al1 , Al2 and Al3) are all six-coordinated and bridged by carboxylate groups, O^{2-} (O9), OH^- (O1H and O10) and H_2O (O1w) groups (Figure 4(e)) to form spiral chains along *c* axis as shown in Figure 4(f). To our knowledge, this spiral shape aluminum oxide chain is a new type of substructural building unit (SBU) for Al-MOFs . In contrast, the zig-zag aluminum oxide chains in **AITCS-1** are planar. Each TCS^{4-} ligand connects with three Al^{3+} chains as shown in Figure S11, forming a 3D framework, showing elliptical channels of $4.6(3.0) \times 9.4(7.7) \text{ \AA}^{[41]}$ (channels shown in *a* and *b* direction), $7.5(5.9)$ and $10.4(8.7) \times 5.8(4.0) \text{ \AA}^{[41]}$ (channels shown in *c* direction) (Figure 4(g) and Figure S10)). It has a large porosity of 57.4% (probing radius: 1.2 \AA), and the solvent accessible volume/unit cell is

4449 Å³ as calculated by the PLATON program.^[16] The pore volume calculated based on the above data is 0.70 cm³/g. Based on the topology analysis using ToposPro program,^[17] the 3D framework of **AITCS-2** can be simplified as a 4-nodal 4,5,6,8-c net (Si₂(Al1)₂(Al2)₂(Al3)) with a point symbol of (3⁴4⁷5¹²6⁵)₂(3⁴4⁵5⁴6²)₂(3³4³5³6)₂(3²4¹5²6) as shown in Figure 4(h). To the best of our knowledge, this is a new topology.

Adsorption properties of AITCS-1 and -2

AITCS-1 absorbed very limited N₂ and H₂ molecules at 77 K as shown in Figure S12, consistent with its small porosity. The Langmuir specific surface area is 12.1 m² g⁻¹ (BET: 11 m² g⁻¹) based on nitrogen adsorption isotherm at 77 K. In the region of P/P₀ > 0.70, the isotherm began to increase sharply, indicating the presence of some textural mesopores.^[18] The H₂ uptake is 29.4 ml g⁻¹ (1.31 mmol g⁻¹, 0.26 wt%) under 1 bar and 77 K. The CO₂ uptakes at 273 and 298 K under 1 atm are 38 and 30 ml g⁻¹ (1.70 and 1.34 mmol g⁻¹; 7.5 and 5.9 wt%), respectively; and increased to 112 and 97 ml/g (5.0 and 4.3 mmol g⁻¹; 22 and 19 wt%) under 9 atm (Figure S12). The CH₄ uptakes at 273 and 298 K under 1 atm are 6.1 and 4.2 ml g⁻¹ (0.27 and 0.19 mmol g⁻¹; 0.44 and 0.30 wt%), respectively; and increased to 35 and 26 ml g⁻¹ (1.56 and 1.16 mmol; 2.5 and 1.9 wt%) under 9 atm. Thus, **AITCS-1** absorbs CO₂ a lot more than CH₄, suggesting it might be applied to remove CO₂ from natural gas. The uptake amount of CO₂ is high considering its low pore volume (0.13 ml g⁻¹).^[19] We observed hysteresis in those sorption experiments (Figure S12). MOFs having pores of diameters less than 10 Å could result in hysteresis phenomena due to their small pore nature as reported by Kim *et al.*^[20]

The permanent porosity of **AITCS-2** has been confirmed by nitrogen and hydrogen sorption experiments at 77 K (Figure 5). The N₂ uptakes is 385 cm³ (STP) g⁻¹. The Brunauer–Emmett–Teller (BET) specific surface area is 1506 m²g⁻¹, the Langmuir surface area is 1642 m²g⁻¹, and the pore volume is 0.55 cm³ g⁻¹. The type I adsorption curve suggests the micropore nature of **AITCS-2**. The H₂ uptake is 201 ml g⁻¹ (1.79 wt%) under 1 bar and 77 K, which is moderate among MOF materials. For example, ZIF-8 (BET: 1630 m² g⁻¹) absorbs 1.27 wt%, MOF-5 (BET: 3362 m² g⁻¹) absorbs 1.32 wt% under 1 bar and 77 K.^[21] The CO₂ and CH₄ uptakes at 298 K and 1 bar are 51 cm³ (STP) g⁻¹ (2.3 mmol g⁻¹, 10 wt%) and 15 cm³ (STP) g⁻¹ (0.67 mmol g⁻¹, 1.1 wt%), respectively. The CO₂ and CH₄ uptakes increase to 92 cm³ (STP) g⁻¹ (4.1 mmol g⁻¹, 18 wt%) and 27 cm³ (STP) g⁻¹ (1.2 mmol g⁻¹, 2.0 wt%) at 273 K and 1 bar. To our knowledge, the CO₂ and CH₄ adsorption capacities of **AITCS-2** are relatively high among the reported values of the known MOFs measured under the same conditions.^[19c, 22] UiO(bpdc) (a Zr-MOF based on 2,2-bipyridine-5,50-dicarboxylate (bpdc) ligand) was recently reported as a material has high CO₂ and CH₄ uptakes.^[23] The CO₂ and CH₄ uptakes of **AITCS-2** are higher than that of UiO(bpdc), which has a much larger BET surface area (2646 m² g⁻¹) and absorbs 8.0 wt% CO₂ or 1.0 wt% CH₄ at 1 bar and 293 K; and 13.0 wt% CO₂ at 1 bar and 273 K.^[23]

IR and Raman Spectra of AITCS-1 and -2

The IR and Raman spectra of **AITCS-1** and **-2** are very

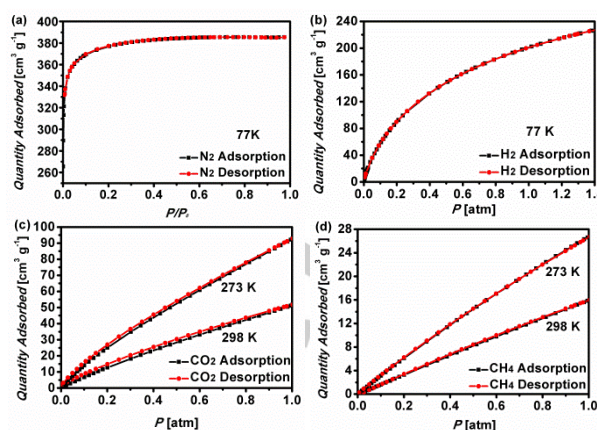


Figure 5. N₂ (77 K), H₂ (77 K), CO₂ (273 and 298 K) and CH₄ (273 and 298 K) adsorption/desorption isotherms of **AITCS-2**.

similar (Figure S14), consistent with the fact that they have similar bonds in the frameworks. When the CuBTC MOF (BTC = 1,3,5-benzene tricarboxylate) was subjected in high humidity environment, the most notable changes in its IR spectra were the gradual appearance of bands at 1708 and 1243 cm⁻¹, which were assigned to the corresponding to the C=O and C–O stretching bands of the COOH group.^[24] Based on this finding, the sharp peak at 3690 cm⁻¹, the strong peaks at 1704 and 1286 cm⁻¹ in the IR spectrum of **AITCS-1** were assigned to the free OH of COOH stretching, the C=O (usually very strong) and C–O stretching modes of COOH group, respectively, which are absent in the IR spectrum of **AITCS-2**, consistent with the fact that **AITCS-2** does not contain -COOH group. Since the IR intensity of $\nu_{\text{sym}}(\text{COO}^-)$ is usually weaker than the IR intensity of $\nu_{\text{asym}}(\text{COO}^-)$, the peaks at around 1610 and 1385 cm⁻¹ in the IR spectra of **AITCS-1** and **-2** were assigned to the $\nu_{\text{asym}}(\text{COO}^-)$ and $\nu_{\text{sym}}(\text{COO}^-)$ modes.

Water and thermal stability of AITCS-1 and -2

Thermogravimetric (TG) curves of **AITCS-1** and **-2** are given in Figure 6. The weight loss of 2.3% (**AITCS-1**) and 2.4% (**AITCS-2**) before 200 °C are due to the adsorbed water molecules. The second weight loss of 6.2% in the TG of **AITCS-1** occurred in the range of 230 to 390 °C corresponds the decomposition of the framework, consistent with the fact that it completely lost crystallinity after being heated at 400 °C for 4 h (Figure 7(a)). However, the PXRD (Figure 7(a)) and IR (Figure S15) studies indicate that the framework kept intact even after being heated at 350 °C for 4 h.

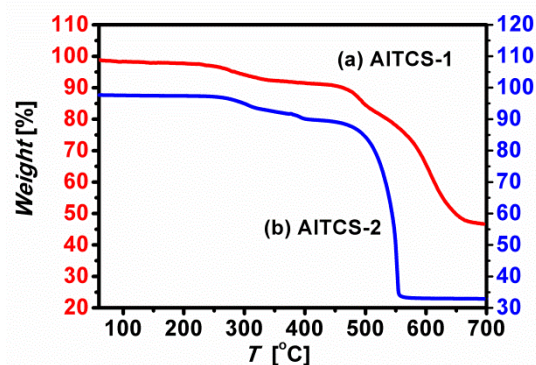


Figure 6. TG curves of **AITCS-1** and **-2**.

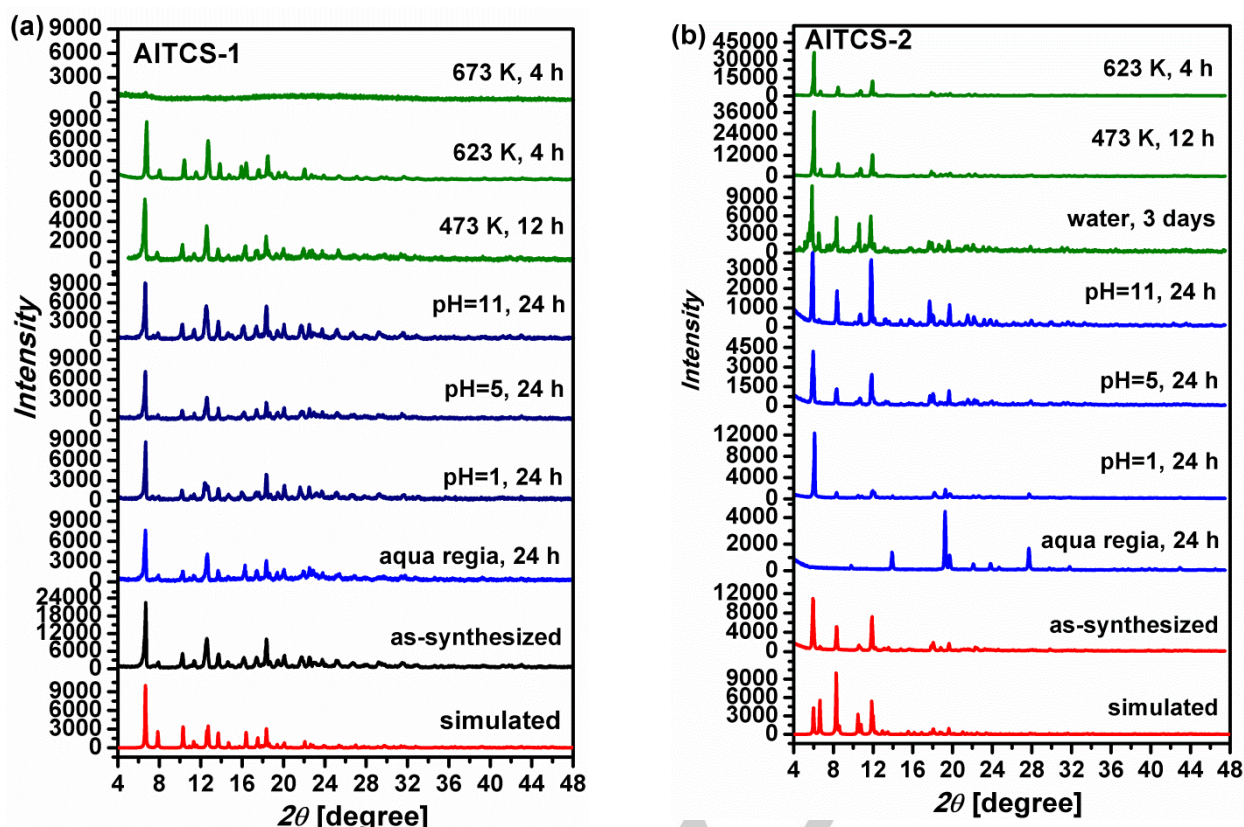


Figure 7. Thermal and water stability of AITCS-1 (a) and AITCS-2 (b) checked by PXRD.

The second weight loss of 3.6% in TG of **AITCS-2** (Figure 6) occurred in the range of 257–320 °C, which was assigned to the loss of the coordinated water (theoretical amount: 2.8%). The PXRD (Figure 7(b)) studies indicate that the framework kept intact even after being heated at 350 °C for 4 h. The IR spectra of the sample heated at 250–350 °C (Figure S15) indicate that **AITCS-2** gradually decomposes at temperatures above 250 °C, suggested by the increase of the peak intensities due to the formation of –COOH group at 1707 (C=O stretching) and 1263 cm^{-1} (C–O stretching) (Figure S15(i)). **AITCS-1** and **-2** can be stable in wide pH range (1–11) for at least 24 h (Figure 7), and **AITCS-1** can even be stable in aqua regia solution for 24 h without the loss of crystallinity as indicated by PXRD pattern (Figure 7) and IR and Raman spectra (Figure S14). In contrast, aqua regia destroys **AITCS-2**. Thus, **AITCS-1** shows greater chemical and thermal stability than **AITCS-2**, which could be due to its low porosity.

UV-Vis diffuse reflectance spectra of AITCS-1, AITCS-2 and the H₄TCS ligand

The UV-Vis diffuse reflectance spectra of H₄TCS, **AITCS-1** and **AITCS-2** in the form of absorption coefficient versus wavelength are given in Figure 8 (The plot of R% versus wavelength are given in Figure S16). The ligand H₄TCS basically only absorbs UV light, while **AITCS-1** and **-2** can absorb visible light and the absorbance of **AITCS-1** is greater than that of **AITCS-2**. The above results demonstrate that Al³⁺, which is not an electron rich ion, could also decrease the band gaps of MOFs to make them absorbing visible light. This function of Al³⁺ has not been recognized. Lu *et al.* proposed that the band gaps of semiconducting MOFs can be decreased by

applying electron-rich metal nodes based on limited experimental and theoretical results.^[1b] A possible explanation for the absorbance difference between **AITCS-1** and **-2** is given below.

A structural motif, namely donor-(π bridge)-acceptor (Organic π -systems end-capped with an electron donor (D) and an electron acceptor (A)) are widely applied in designing efficient organic dyes applied in Dye Sensitized Solar Cell (DSSC).^[25] Due to the D–A interaction, or the so-called intramolecular charge-transfer (ICT), a new low-energy molecular orbital (MO) is being formed. Facile excitation of the electrons within the new MO can be achieved using visible light.^[25c] For example, whereas aniline and nitrobenzene only absorbs in the UV region, 4-nitroaniline showed intense and bathochromically shifted long-wavelength absorption maxima (CT-band), and absorbs in the visible light region. On the contrary, 3-nitroaniline showed only a diminished CT-band as a result of a non-conjugating arrangement of the amino donor and the nitro acceptor.^[25c] **AITCS-1** can be viewed as a D- π -A system due to its unsymmetrical structure caused by its carboxyl groups. –SiR₃ can be seen as the electron donor; phenyl ring is the π bridge; and the –COOH is the electron acceptor, thus it starts to absorb visible light. In contrast, the symmetric structure of **AITCS-2** makes it not a D- π -A system. Consistently, it absorbs little visible light.

The band gaps of materials can be calculated by the following equation:^[26]

$$\alpha h\nu = A(h\nu - E_g)^{n/2}$$

Where α , ν , E_g , and A are absorption coefficient, light frequency, band gap, and a constant, respectively. n is determined by the optical transition type of the semiconductor (i.e., n equals 1 for direct allowed transition and 4 for indirect forbidden transition)^[26a] Because α is

proportional to $F(R)$ ($F(R)$ equals $(1-R)^2/(2R)$ where R is the reflectance in the UV-Vis diffuse reflectance spectra.),^[26c, 26d] the energy intercept of a plot of $(F(R)h\nu)^2$ versus energy ($h\nu$) yields E_g for a direct allowed transition when the linear region is extrapolated to zero coordinate, and the energy intercept of a plot of $(F(R)h\nu)^{1/2}$ versus energy ($h\nu$) yields E_g for an indirect allowed transition. The bandgaps of **AITCS-1** and **-2** are determined as 2.59 and 2.72 eV, respectively, assuming they are indirect bandgap semiconductor or 3.10 or 3.59 eV, respectively, assuming they are direct bandgap semiconductors (Figure S16(b)).

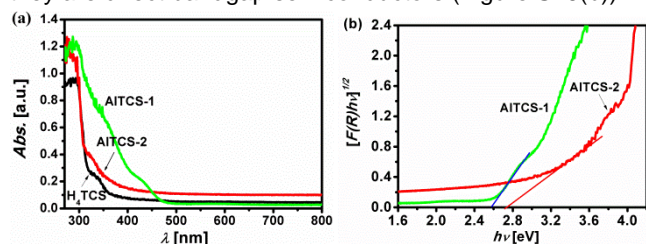


Figure 8. Optical properties of **AITCS-1** and **-2**. (a) UV-Vis reflectance spectra of H_4TCS , **AITCS-1** and **-2** in the form of absorbance versus wavelength; (b) The bandgaps of **AITCS-1** and **-2** determined by the plotting of $(F(R)h\nu)^{1/2}$ versus $h\nu$.

Determination of band gaps and conduction and valence band edges of **AITCS-1** and **-2** by an electrochemical method

To figure out whether they are direct or indirect bandgap semiconductors, the conduction-band (CB) edge (LUMO) and valence-band (VB) edge (HOMO) positions of materials were also determined by an electrochemical method, i.g. the linear potential scan method which can be viewed as partial cyclic voltammetry curves. This method is well established in the literature.^[27] The first oxidation potential (E_{ox}) and the first reduction potential (E_{red}) can be observed by the separate cathodic and anodic scans, respectively, and equals to the energy levels of the HOMO (the conduction band edge) and LUMO (the valence band edge) of the material, respectively. The bandgap is the difference of E_{ox} and E_{red} . However, sometimes not both potentials were observed,^[27c] which is probably due to the redox reactions of the electrolytes during the processes. We therefore, different from the literatures, used two different electrolytes (the phosphate buffered saline (PBS, 0.1 M, pH=7.4) solution and a H_2SO_4 aqueous solution (pH = 5.01)), so that we could observe both redox potentials and crosscheck the results.^[28] When determining the band edges, the current curves (in red) of the electrolytes obtained using unmodified ITO electrodes under same scan conditions were compared with the observed current curves obtained using the modified ITO electrodes as shown in Figure 9 (**AITCS-1**) and Figure S2 (**AITCS-2**) in order to distinguish the redox positions of the materials from those of the electrolytes. As shown in Figure 9, the VB band edge of **AITCS-1** (1.48 V) was more obviously observed in the anodic scan using the PBS (PBS, 0.1 M, pH=7.4) solution, and the CB band edge of **AITCS-1** (-1.06 V) was more obviously observed in the cathodic scan using the pH = 5.01 H_2SO_4 aqueous solution. The VB band edge of **AITCS-2** (1.58 V) was found in the anodic scan using the PBS (0.1 M, pH=7.4) solution, and the CB band edge of **AITCS-2** (-0.96 V) was found in the cathodic scan using the

pH = 5.01 H_2SO_4 aqueous solution (Figure S2). That is, the CB and VB potentials of **AITCS-1** and **AITCS-2** are -0.86 and 1.68 V; -0.76 and 1.78 versus the normal hydrogen electrode (NHE), respectively and the band gaps of both **AITCS-1** and **-2** were found both to be 2.54 by the EC method, which is very close to the values determined based on UV-Vis reflectance spectra assuming they are indirect bandgap semiconductors, indicating that both **AITCS-1** and **-2** are indirect band gap semiconductors.

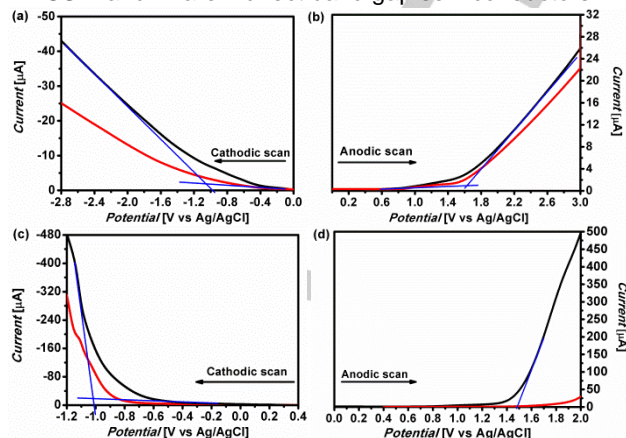


Figure 9. Cathodic and anodic linear potential scans for determining the positions of the conduction band (CB) and valence band (VB) edges of **AITCS-1** using two different electrolytes. The red curves are the currents of the electrolytes using the unmodified ITO electrodes ((a)-(b): the pH = 5.01 H_2SO_4 aqueous solution, (c)-(d): a phosphate buffered saline (PBS, 0.1 M, pH=7.4)).

Photoelectric properties of **AITCS-1** and **-2**

The photoelectrical properties of **AITCS-1** and **-2** were studied in a three-electrode set-up. Rapid and stable photocurrent responses of **AITCS-1** and **-2** under UV and visible light illuminations are observed (Figure 10). The anodic photocurrent response indicates the n-type semiconductor characteristic of these two materials.^[29] The current increases upon irradiation at shorter wavelength, which is consistent with the higher light absorbances of **AITCS-1** and **-2** at shorter wavelength compared to those at longer wavelength. Similar phenomenon was also reported by Ardo *et al.*^[30] The generated photocurrent increases with increasing applied bias potential. Such phenomena of other materials were also observed by Liu and Zhang *et al.*^[31] The photocurrent densities of **AITCS-1** and **-2** reaches 100 and 60 $nAcm^{-2}$, respectively at 0.6 V (vs. Ag/AgCl). A higher photocurrent density often means a higher ability in separating the photogenerated electrons and holes.^[29b, 32] The above results suggest that faster recombinations of photogenerated electrons and holes occur under lower potential bias.^[33] Under the same condition, the photocurrent intensity increases in the order of **AITCS-2** < **AITCS-1**, consistent with the fact that **AITCS-1** absorbs more UV light and visible light than **AITCS-2**, which suggested that **AITCS-1** had a more efficient separation for the photogenerated electron-hole pairs.^[32b]

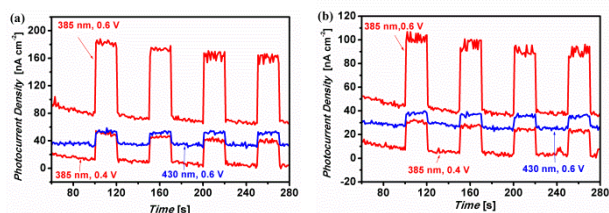


Figure 10. AITCS-1(a) and -2(b) illuminated with 385 and 430 nm light at 0.4 and 0.6 V.

Photocatalytic water splitting using AITCS-1

The CB and VB band-edge positions suggest that **AITCS-1** and **-2** could have application as visible light photocatalysts for water splitting based on the known photocatalytic mechanism,^[34] since the positions of redox potentials of neutral water is -0.41 and 0.82 V for $E^0(\text{H}^+/\text{H}_2)$ and $E^0(\text{O}_2/\text{H}_2\text{O})$, respectively. However no photocatalytic water splitting properties of **AITCS-1** and **-2** were observed in neutral water under visible light, probably due to the low visible light absorbance and poor photogenerated charge (electrons and holes) separation efficiencies. When 10 mg **AITCS-1** (synthesized by the typical synthesis of **AITCS-1** which applied a rather slow cooling rate) was put into a mixed solvent of water and triethanolamine (TEOA) (4:1 volume ratio, pH = 11.0, 100 mL), the evolved hydrogen reaches the maximum 500 $\mu\text{mol/g}$ after 10 h with an average rate of 50 $\mu\text{mol}\cdot\text{g}^{-1}\cdot\text{h}^{-1}$ under visible light (420-800 nm). TEOA acts as a sacrificial electron donor, and the reduction potential of $E^0(\text{TEOA}^+/\text{TEOA})$ equals 0.82 (Eq. (3)).^[35] TEOA molecules donate electrons to the valence band to eliminate the holes generated by visible light and thus increase the charge separation efficiency (Figure 10b). The reduction potential of $E^0(\text{H}^+/\text{H}_2)$ at pH = 11.0 is -0.65 V, thus the photogenerated electrons in the conduction band of the **AITCS-1** can reduce H^+ into H_2 as shown in Figure 11(b). The kinetics of the half reaction, in which H_2O donates electrons to the conduction band and itself is oxidized to O_2 (Eq. (2)) is rather slow and was not observed. The amount of evolved hydrogen decreases after 10 h, which is probably due to the gradual deterioration of **AITCS-1** as indicated by the decreased crystallinity of the recovered solid shown by its PXRD pattern (Figure S17). Since every hour a portion of gas in the reaction vessel would be extracted to be analyzed, when the hydrogen production is too slow or stops, the apparent hydrogen production would decrease. Under the same reaction condition as that of **AITCS-1**, **AITCS-2** did not show photocatalytic water splitting property under visible light, probably due to its very low visible light absorbance, and no hydrogen observed also under UV light (300 W Xe lamp without using filter).

The hydrogen evolution efficiency of **AITCS-1** is better than the efficiency of the rhodamine B/UiO-66(Zr) reported by Wang and Yan et al.,^[36] which reaches the maximum (170 $\mu\text{mol/g}$, 34 $\mu\text{mol}\cdot\text{g}^{-1}\cdot\text{h}^{-1}$) after 5 h under similar reaction conditions. However, it is less efficient than that of **AI-PMOF**^[2] [$\text{Al}_2(\text{OH})_2(\text{H}_2\text{TCCP})$] (200 $\mu\text{mol}\cdot\text{g}^{-1}\cdot\text{h}^{-1}$, H_2TCCP = meso-tetra(4-carboxyl-phenyl) porphyrin,) and that of MOF-253-Pt^[37] (4680 $\mu\text{mol}\cdot\text{g}^{-1}\cdot\text{h}^{-1}$, MOF-253: $\text{Al}(\text{OH})(\text{bpydc})$, bpydc = 2,2'-bipyridine-5,5'-dicarboxylate) under visible light. To our knowledge, one of the best performance of MOF related materials is the $\text{MoS}_2/\text{UiO-66}/\text{CdS}$ composite which could produce 32500 $\mu\text{mol}\cdot\text{g}^{-1}\cdot\text{h}^{-1}$

hydrogen under visible light. Bao *et al.* reported that a nanocrystalline CoO photocatalyst can carry out overall water splitting with a hydrogen production efficiency of 71,429 $\mu\text{mol}\cdot\text{g}^{-1}\cdot\text{h}^{-1}$ without using sacrificial agent under the illumination of an AM 1.5G solar simulator.^[38] To our knowledge, one of the best performance of non-MOF containing material is the $\text{Ni}_n\text{-CdSe}/\text{CdS}$ core/shell QDs which could produce 153 $\text{mmol}\cdot\text{g}^{-1}\cdot\text{h}^{-1}$ hydrogen under visible light,^[38b, 39] and one of the best TiO_2 containing material is the carbon/ TiO_2 /CNTs composite which could a hydrogen evolution efficiency of 37600 $\mu\text{mol}\cdot\text{g}^{-1}\cdot\text{h}^{-1}$ under the light of an AM 1.5G solar simulator.^[38b, 40] Although the photocatalytic water splitting property of **AITCS-1** is far inferior to the above materials, it is the first report on the photocatalytic water splitting property of crystals of an Al-MOF.



(E° is the reduction potential in pH = 11.0 aqueous solution)

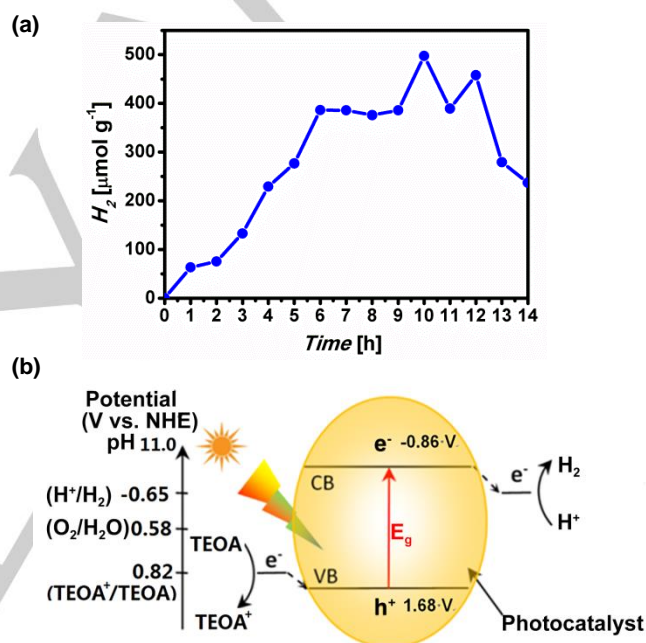


Figure 11. (a) Photocatalytic H_2 evolution amounts for **AITCS-1** (synthesized by the typical synthesis of **AITCS-1**) as a function of light irradiation time, (b) Proposed mechanism of the photocatalytic water splitting process of **AITCS-1** in a 4:1 volume ratio mixed solvent (100 mL, pH = 11.0) solution of H_2O and TEOA.

Conclusions

We demonstrated how to grow high quality, large single crystal aluminum carboxylate MOFs in three cases, resulting in two novel Al-MOFs, **AITCS-1** and **-2**. Based on our experiences, we proposed an efficient method of preparing large and good quality single crystals of Al-MOFs. The method includes the incorporation of three techniques: 1) Adding a simple inorganic or organic acid (e.g. HF or formic acid); 2) Applying an efficient experimental method, i.g. the orthogonal array design approach; 3) Using PXRD to check the crystallinity and identity of the product during the investigation process. Good quality open framework Al-MOF single crystals should usually have a PXRD

pattern which has a peak at a 2θ angle lower than 10° , high crystallinity and sharp peaks. In addition, we found changing solvent polarity and faster cooling rate are favorable to synthesize good quality large single crystals. This method is possibly also useful to synthesize other MOF single crystals. In addition, **AITCS-1** and **-2** are the first examples of Al-MOFs synthesized based on a tetrahedral shape ligand. **AITCS-2** is also the first Al-MOF which contains a spiral chain SBU. **AITCS-1** and **-2** can be stable in wide pH range (1-11), and **AITCS-1** can even be stable in aqua regia solution. We also found that Al^{3+} , not electron rich ions, could transform a UV light absorbing ligand (i.g. H_4TCS) to absorb visible light, which has not been recognized before.

Experimental Section

Synthesis of the MIL-53(Al) single crystal

In a typical synthesis, H_2BDC (0.3456 g, 2.080 mmol), $\text{Al}(\text{NO}_3)_3 \cdot 9\text{H}_2\text{O}$ (1.56 g, 4.160 mmol), hydrofluoric acid (403 μL , 9.11 mmol, 40% aq.) and H_2O (6.0 mL, 330 mmol) were stirred for 10 min in a 14 ml glass vial (diameter: 2.0 cm, height: 5.6 cm). The overall molar ratio of $\text{Al}(\text{NO}_3)_3$: H_2BDC : HF: H_2O = 2.0: 1: 4.4 : 160. The glass vial was then sealed in an autoclave equipped with a Teflon liner (25 mL) and put into an oven. The oven was heated up to 220°C over 1 h, kept at this temperature for 3 d, and then turned off. The autoclave was cooled down to room temperature naturally in the oven, resulted in colourless block crystals (Figure 1(c)) and white powders. The single-crystal X-ray diffraction analysis was carried out on one of the block crystal, the simulated PXRD spectrum of which is given in Figure S1(b). The product was dried in an oven for 12 h at $70\text{--}90^\circ\text{C}$, the PXRD pattern (25°C) of which is shown in Figure S3(g). In a separate preparation, the crystals were separated from the white powders utilizing their density difference, and dried in an oven at $70\text{--}90^\circ\text{C}$ for 12 h, the PXRD pattern of which is shown in Figure S3(h).

Synthesis of $[\text{Al}_3(\text{OH})_3(\text{HTCS})_2]$ (**AITCS-1**)

In a typical synthesis using HF aqueous solution, H_4TCS (0.040 g, 0.078 mmol), $\text{Al}(\text{NO}_3)_3 \cdot 9\text{H}_2\text{O}$ (468 μL , 1.0 M $\text{Al}(\text{NO}_3)_3 \cdot 9\text{H}_2\text{O}$ aqueous solution, 0.468 mmol), hydrofluoric acid (80 μL , 10% aqueous solution, 4.1 mmol), and H_2O (8.0 mL, 444 mmol) were stirred for 10 min in a 14 ml glass vial. The overall molar ratio of $\text{Al}(\text{NO}_3)_3$: H_4TCS : HF: H_2O = 6.0 : 1 : 5.3 : 5700. The glass vial was then sealed in an autoclave equipped with a Teflon liner (25 mL) and put into an oven. The temperature of the oven was raised from room temperature to 220°C with a $1.0^\circ\text{C}/\text{min}$ heating ramp, kept at 220°C for 3 d, and then cooled to 120°C with a rate of $1.0^\circ\text{C}/\text{h}$, and to 25°C with a rate of $10^\circ\text{C}/\text{h}$. The resulted colourless block crystals (when grounded to powder, showing light yellow colour) were collected by filtration, and washed with DMF and then with H_2O and dried in a 90°C oven for 12 h. The overall yield is 39 mg, 78 wt% based on H_4TCS . Its purity was checked by PXRD (Figure 7). IR (KBr): $\tilde{\nu}$ = 3685 (w) ($\nu(\text{O-H})$ of COOH), 3425 (w), 3020 (w), 2659 (w), 2536 (w), 1948 (w), 1704 (s) ($\nu(\text{C=O})$ of COOH), 1625 (s) ($\nu_{\text{asym}}(\text{COO}^-)$), 1589 (s), 1540 (s), 1503 (s), 1439 (vs), 1385 (s) ($\nu_{\text{sym}}(\text{COO}^-)$), 1135 (w), 1318 (w), 1286 (m) ($\nu(\text{C-O})$ of COOH), 1255 (w), 1192 (w), 1099 (s), 1022 (w), 995 (m), 971 (m), 904 (w), 856 (w), 781 (s), 733 (s), 709 (s), 633 (m), 611 (m), 564 (w), 505 (s), 474 (w), 452 (w), 413 (w) cm^{-1} ; elemental analysis calcd (%) for $[\text{Al}_3(\text{OH})_3(\text{HTCS})_2](\text{DMF})_{0.25}(\text{H}_2\text{O})$: C 57.41, H 3.46, N, 0.29; found: C 57.48, H 3.42, N 0.29. In the syntheses of **AITCS-1** using HCOOH reagent, the heating procedure is as that of the syntheses of MIL-53(Al) single crystals. The amounts of H_4TCS and H_2O are 10 mg (0.020 mmol) and 6.0 mL (333 mmol), respectively.

Synthesis of $[\text{Al}_5\text{O}_2(\text{OH})_3(\text{TCS})_2(\text{H}_2\text{O})_2]$ (**AITCS-2**)

In an optimized preparation for the best quality single crystals of **AITCS-2**, H_4TCS (0.020 g, 0.039 mmol), $\text{Al}(\text{NO}_3)_3 \cdot 9\text{H}_2\text{O}$ (227 μL , 1.0 M $\text{Al}(\text{NO}_3)_3 \cdot 9\text{H}_2\text{O}$ aqueous solution, 0.227 mmol), formic acid (0.40 mL, 10.6 mmol), DMF (N,N-dimethylformamide, 1.4 mL, 18.2 mmol) and H_2O (0.6 mL, 33.3 mmol) were stirred for 10 min in a 14 mL glass vial. The overall molar ratio of $\text{Al}(\text{NO}_3)_3$: H_4TCS : HCOOH : DMF : H_2O = 6.0 : 1 : 270 : 470 : 850. The glass vial was then sealed in an autoclave equipped with a Teflon liner (25 mL) and put into an oven. The temperature of the oven was raised to 120°C naturally, kept at 120°C for 3 d, and then cooled to 25°C naturally, resulting in colourless block-like crystals. The crystals were collected by filtration, washed with DMF and then with H_2O and dried in a 90°C oven for 12 h. The overall yield is 16.2 mg, 63 wt% based on H_4TCS . The PXRD was obtained and shown in Figure 2 no 14. IR (KBr): $\tilde{\nu}$ = 3451 (w, br) ($\nu(\text{O-H})$ of absorbed H_2O), 1707 (w), 1620 (s) ($\nu_{\text{asym}}(\text{COO}^-)$), 1595 (s), 1546 (s), 1506 (s), 1443 (s), 1390 (w) ($\nu_{\text{sym}}(\text{COO}^-)$), 1315 (w), 1259 (w), 1191 (w), 1105 (s), 1021 (m), 976 (w), 957 (w), 857 (s), 777 (s), 741 (s), 729 (s), 710 (m), 631 (m), 610 (m), 556 (m), 507 (m), 460 (w); elemental analysis calcd (%) for $[\text{Al}_5\text{O}_2(\text{OH})_3(\text{TCS})_2(\text{H}_2\text{O})_2](\text{H}_2\text{O})_6$ (Sample was washed thoroughly with H_2O and dried over 120°C for 12 h before measurement.): C 48.77, H 3.73, N 0.0; found: C 48.56, H 3.35, N, 0.00.

X-ray crystallography

Suitable single crystals were selected for single crystal X-ray diffraction. The data were collected at 296 (2) (**AITCS-1**) and 291 (2) K (MIL-53) and 150 (2) K (**AITCS-2**) on a Bruker Smart CCD diffractometer with graphite-monochromatic $\text{K}\alpha$ radiation ($\lambda = 0.71073 \text{ \AA}$) from an enhanced optic X-ray tube. Raw data for the structure were obtained using SAINT, and absorption correction was applied using SADABS programs. The structures of **AITCS-1** and MIL-53 were solved by direct methods and refined by full matrix least-squares on F^2 , using the SHELXS-2014 and SHELXL-2014 programs. The structure of **AITCS-2** were solved by intrinsic phasing method and refined by full matrix least-squares on F^2 , using the SHELXT-2014 and SHELXL-2016 programs. A summary of the crystallographic data, data collection, and refinement parameters for complex is provided in Table S3 (ESI). Selected bond distances and angles are given in Table S4 (ESI).

Acknowledgements

We thank National Natural Science Foundation of China (NSFC) (No. 21622104, 21371099, 21471080, 21071082 and 21671003), the Key International (Regional) Joint Research Program of NSFC (No.21420102002), the Natural Science Foundation of Jiangsu Province (BK20161553), the Natural Science Foundation of Education Department of Jiangsu Province (No. 16KJB150021), the Priority Academic Program Development of Jiangsu Higher Education Institutions, and the Foundation of Jiangsu Collaborative Innovation Center of Biomedical Functional Materials for their funding support.

Keywords: single crystal • Al(III) metal-organic framework • water splitting • visible light • semiconductor

- [1] a) S. Wang, X. Wang, *Small* **2015**, *11*, 3097-3112; b) M. Usman, S. Mendiratta, K.-L. Lu, *Adv. Mater.* **2016**, *29*, 1605071.
- [2] A. Fateeva, P. A. Chater, C. P. Ireland, A. A. Tahir, Y. Z. Khimyak, P. V. Wiper, J. R. Darwent, M. J. Rosseinsky, *Angew. Chem. Int. Ed.* **2012**, *51*, 7440-7444; *Angew. Chem.* **2012**, *124*, 7558-7562.

- [3] M. Gaab, N. Trukhan, S. Maurer, R. Gummaraju, U. Mueller, *Micropor. Mesopor. Mater.* **2012**, *157*, 131-136.
- [4] U. Mueller, G. Luinstra, O. M. Yaghi, in *BASF Aktiengesellschaft, Vol. US Pat. 6 617 467* **2004**.
- [5] E. Alvarez, N. Guillou, C. Martineau, B. Bueken, B. Van de Voorde, C. Le Guillouzer, P. Fabry, F. Nouar, F. Taulelle, D. de Vos, J.-S. Chang, K. H. Cho, N. Ramsahye, T. Devic, M. Daturi, G. Maurin, C. Serre, *Angew. Chem. Int. Ed.* **2015**, *54*, 3664-3668; *Angew. Chem.* **2015**, *127*, 3735-3739.
- [6] T. Loiseau, L. Lecroq, C. Volkringer, J. Marrot, G. Ferey, M. Haouas, F. Taulelle, S. Bourrelly, P. L. Llewellyn, M. Latroche, *J. Am. Chem. Soc.* **2006**, *128*, 10223-10230.
- [7] C. G. Wang, J. X. Wu, M. C. Hu, N. Li, N. J. Guan, S. H. Xiang, *J. Porous Mat.* **2012**, *19*, 751-759.
- [8] Y. Han, M. Liu, K. Li, Y. Zuo, Y. Wei, S. Xu, G. Zhang, C. Song, Z. Zhang, X. Guo, *Crystengcomm* **2015**, *17*, 6434-6440.
- [9] Y. Bai, Y. Dou, L.-H. Xie, W. Rutledge, J.-R. Li, H.-C. Zhou, *Chem. Soc. Rev.* **2016**, *45*, 2327-2367.
- [10] B. Seoane, S. Sorribas, Á. Mayoral, C. Téllez, J. Coronas, *Micropor. Mesopor. Mater.* **2015**, *203*, 17-23.
- [11] O. L. K. Davies, *Design and Analysis of Industrial Experiments*, 2nd ed. ed., Longman Group Limited, London and New York, **1978**.
- [12] J. Luo, G. Zhu, F. Zhang, Q. Li, T. Zhao, X. Zhu, *Rsc Adv.* **2015**, *5*, 6071-6078.
- [13] C.-S. Tsao, M.-S. Yu, T.-Y. Chung, H.-C. Wu, C.-Y. Wang, K.-S. Chang, H.-L. Chent, *J. Am. Chem. Soc.* **2007**, *129*, 15997-16004.
- [14] B. Chen, X. J. Wang, Q. F. Zhang, X. Y. Xi, J. J. Cai, H. Qi, S. Shi, J. Wang, D. Yuan, M. Fang, *J. Mater. Chem.* **2010**, *20*, 3758-3767.
- [15] Z.-W. Wang, M. Chen, C.-S. Liu, X. Wang, H. Zhao, M. Du, *Chem. Eur. J.* **2015**, *21*, 17215-17219.
- [16] A. L. Spek, *Acta Cryst.* **2009**, *D65*, 148-155.
- [17] V. A. Blatov, A. P. Shevchenko, D. M. Proserpio, *Cryst. Growth Des.* **2014**, *14*, 3576-3586.
- [18] C. Chen, D.-W. Park, W.-S. Ahn, *Appl. Surf. Sci.* **2014**, *292*, 63-67.
- [19] a) Z. Zhang, Y. Zhao, Q. Gong, Z. Li, J. Li, *Chem. Commun.* **2013**, *49*, 653-661; b) R. Sabouni, H. Kazemian, S. Rohani, *Environ. Sci. Pollut. Res.* **2014**, *21*, 5427-5449; c) K. Sumida, D. L. Rogow, J. A. Mason, T. M. McDonald, E. D. Bloch, Z. R. Herm, T. H. Bae, J. R. Long, *Chem. Rev.* **2012**, *112*, 724-781.
- [20] J. Kang, S.-H. Wei, Y.-H. Kim, *J. Am. Chem. Soc.* **2010**, *132*, 1510-1511.
- [21] a) J. Sculley, D. Yuan, H.-C. Zhou, *Energ. Environ. Sci.* **2011**, *4*, 2721-2735; b) M. P. Suh, H. J. Park, T. K. Prasad, D. W. Lim, *Chem. Rev.* **2012**, *112*, 782-835.
- [22] T. A. Makal, J.-R. Li, W. Lu, H.-C. Zhou, *Chem. Soc. Rev.* **2012**, *41*, 7761-7779.
- [23] L. Li, S. Tang, C. Wang, X. Lv, M. Jiang, H. Wu, X. Zhao, *Chem. Commun.* **2014**, *50*, 2304-2307.
- [24] J. B. DeCoste, G. W. Peterson, B. J. Schindler, K. L. Killops, M. A. Browe, J. J. Mahle, *J. Mater. Chem. A* **2013**, *1*, 11922-11932.
- [25] a) A. Yella, C.-L. Mai, S. M. Zakeeruddin, S.-N. Chang, C.-H. Hsieh, C.-Y. Yeh, M. Graetzel, *Angew. Chem. Int. Ed.* **2014**, *53*, 2973-2977; *Angew. Chem.* **2014**, *126*, 3017-3021; b) J. N. Clifford, E. Martinez-Ferrero, A. Viterisi, E. Palomares, *Chem. Soc. Rev.* **2011**, *40*, 1635-1646; c) F. Bures, *Rsc Adv.* **2014**, *4*, 58826-58851.
- [26] a) M. A. Butler, *J. Appl. Phys.* **1977**, *48*, 1914-1920; b) G. Q. Zhang, W. Wang, Q. X. Yu, X. G. Li, *Chem. Mater.* **2009**, *21*, 969-974; c) Z. Sha, J. Wu, *Rsc Adv.* **2015**, *5*, 39592-39600; d) A. E. Morales, E. S. Mora, U. Pal, *Revista Mexicana De Física S* **2007**, *53*, 18-22.
- [27] a) G.-L. Wang, J.-X. Shu, Y.-M. Dong, X.-M. Wu, W.-W. Zhao, J.-J. Xu, H.-Y. Chen, *Anal. Chem.* **2015**, *87*, 2892-2900; b) T.-F. Yeh, S.-J. Chen, C.-S. Yeh, H. Teng, *J. Phys. Chem. C* **2013**, *117*, 6516-6524; c) Z. Fang, A. A. Eshbaugh, K. S. Schanze, *J. Am. Chem. Soc.* **2011**, *133*, 3063-3069.
- [28] a) X. Yang, Y. Zhang, F. Li, T. Guo, Y. Wu, F. Jin, M. Fang, Y. Lan, Y. Li, Y. Zhou, Z. Zou, *Dalton Trans.* **2017**, *46*, 8204-8218; b) T. Guo, X. Yang, R. Li, X. Liu, Y. Gao, Z. Dai, M. Fang, H.-K. Liu, Y. Wu, *J. Solid State Chem.* **2017**, *253*, 129-138.
- [29] a) H. Yang, L. Wang, D. Hu, J. Lin, L. Luo, H. Wang, T. Wu, *Chem. Commun.* **2016**, *52*, 4140-4143; b) T. Wu, Q. Zhang, Y. Hou, L. Wang, C. Mao, S.-T. Zheng, X. Bu, P. Feng, *J. Am. Chem. Soc.* **2013**, *135*, 10250-10253.
- [30] W. White, C. D. Sanborn, R. S. Reiter, D. M. Fabian, S. Ardo, *J. Am. Chem. Soc.* **2017**, DOI:10.1021/jacs.7b00974.
- [31] J. Gao, J. Miao, Y. Li, R. Ganguly, Y. Zhao, O. Lev, B. Liu, Q. Zhang, *Dalton Trans.* **2015**, *44*, 14354-14358.
- [32] a) W. Wang, J. Fang, S. Shao, M. Lai, C. Lu, *Appl. Catal. B-Environ.* **2017**, *217*, 57-64; b) J. Liu, R. Li, Y. Hu, T. Li, Z. Jia, Y. Wang, Y. Wang, X. Zhang, C. Fan, *Appl. Catal. B-Environ.* **2017**, *202*, 64-71; c) Y. Fan, Y. Cui, G.-D. Zou, R.-H. Duan, X. Zhang, Y.-X. Dong, H.-T. Lv, J.-T. Cao, Q.-S. Jing, *Dalton Trans.* **2017**, *46*, 8057-8064.
- [33] Y. An, H. Li, Y. Liu, B. Huang, Q. Sun, Y. Dai, X. Qin, X. Zhang, *J. Solid State Chem.* **2016**, *233*, 194-198.
- [34] W. G. Tu, Y. Zhou, Z. G. Zou, *Adv. Mater.* **2014**, *26*, 4607-4626.
- [35] P. Chowdhury, H. Gornaa, A. K. Ray, *Chemosphere* **2015**, *121*, 54-61.
- [36] J. He, J. Wang, Y. Chen, J. Zhang, D. Duan, Y. Wang, Z. Yan, *Chem. Commun.* **2014**, *50*, 7063-7066.
- [37] a) T. Zhou, Y. Du, A. Borgna, J. Hong, Y. Wang, J. Han, W. Zhang, R. Xu, *Energ. & Environ. Sci.* **2013**, *6*, 3229-3234; b) W. Wang, X. Xu, W. Zhou, Z. Shao, *Adv. Sci* **2017**, 1600371.
- [38] a) L. Liao, Q. Zhang, Z. Su, Z. Zhao, Y. Wang, Y. Li, X. Lu, D. Wei, G. Feng, Q. Yu, X. Cai, J. Zhao, Z. Ren, H. Fang, F. Robles-Hernandez, S. Baldelli, J. Bao, *Nat. Nanotechnol.* **2014**, *9*, 69-73; b) X. Li, J. Yu, J. Low, Y. Fang, J. Xiao, X. Chen, *J. Mater. Chem. A* **2015**, *3*, 2485-2534.
- [39] Z.-J. Li, J.-J. Wang, X.-B. Li, X.-B. Fan, Q.-Y. Meng, K. Feng, B. Chen, C.-H. Tung, L.-Z. Wu, *Adv. Mater.* **2013**, *25*, 6613-6618.
- [40] C. Zhao, H. Luo, F. Chen, P. Zhang, L. Yi, K. You, *Energ. & Environ. Sci.* **2014**, *7*, 1700-1707.
- [41] We measured atom to atom distances and then deducted the related covalent radii or van der Waals radii (in parentheses) of the related atoms.

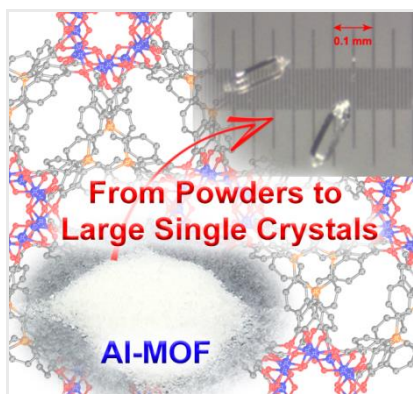
Entry for the Table of Contents (Please choose one layout)

Layout 1:

FULL PAPER

Text for Table of Contents

The first two tetrahedral ligand based, visible light absorbing aluminum carboxylate MOFs (**AITCS-1** and **-2**) based on H₄TCS were synthesized and fully characterized including their water splitting photocatalytic properties; the successful syntheses of large single crystals of **AITCS-1** and **-2** and MIL-53(Al) demonstrate a general method of obtaining single crystals of Al-MOFs large enough for common structure determinations.



Yuanyuan Guo, Jun Zhang, Long-Zhang Dong, Qi Li, Tao Chen, Yan Xu, Wei Han, Min Fang, * Hong-Ke Liu, Yong Wu, * Ya-Qian Lan*

Page No. – Page No.

Syntheses of Exceptionally Stable Al(III) Metal-Organic Frameworks: How to Grow High Quality Large Single Crystals?